Iranian Society of Acoustics and Vibration
The 15th ISAV2025 International Conference on Acoustics and Vibration
24-25 Dec 2025 Tehran- Iran

Material-Based Comparative Design and Simulation of Underwater Ultrasound Acoustic Metamaterial Luneburg Lenses

Mohammad Naeim Moradi[a], Maryam Ghassabzadeh Saryazdi[b*], Abdolreza Ohadi[c]

[a] *PhD student, Acoustics Research Laboratory, Mechanical Engineering Department, Amirkabir University of Technology (Tehran Polytechnic), Tehran, Iran.*

[b] *Assistant Professor, Vehicle Technology Research Institute, Amirkabir University of Technology (Tehran Polytechnic), Tehran, Iran.*

[c] *Professor, Acoustics Research Laboratory, Mechanical Engineering Department, Amirkabir University of Technology (Tehran Polytechnic), Tehran, Iran.*

* Corresponding author e-mail: mghsaryazdi@aut.ac.ir

Abstract

Acoustic metamaterial Luneburg lenses are an important group of gradient refractive index acoustic lenses designed for accurate wave focusing. In recent years, researchers have explored various 2D and 3D Luneburg lens structures with unique unit cell designs. However, a lack of comparative and material driven designs of acoustic metamaterial lenses is noticeable, particularly regarding how using different materials for established unit cells affects focusing behaviour of the acoustic metamaterial lenses. Therefore, this article presents four underwater acoustic metamaterial Luneburg lenses, designed and simulated for working frequency of 40 *kHz* using four common 3D-printing materials: PLA, ABS, PETG and Nylon. The lenses are formed by cubic polymer unit cells with air inclusions acting as acoustic scatterers. Finite element simulations in COMSOL are performed to calculate the dispersion curves and refractive indices of the unit cells with varying filling factors. The unit cells are then arranged next to each other according to the general case of the Luneburg lens profile where the incoming waves are focused at a point on the boundary of the lens. The performance of these lenses is then evaluated by numerical simulations. The results of this study showed that the lenses made of Nylon and PLA successfully achieved the intended high intensity focal point with Nylon lens producing the highest pressure peak of 2.75 times the incident pressure amplitude and PLA lens achieving the narrowest full width at half maximum (FWHM) of 0.57λ. However, the lenses made of ABS and PETG failed to focus the incoming waves onto the predetermined focal point. The findings of this study provide a comparative understanding for designing acoustic metamaterial lenses which have a wide range of applications from industrial to medical fields.

Keywords: Acoustic metamaterials; Luneburg Lens; Underwater Acoustics; Ultrasound.

---

1. Introduction

Acoustic metamaterials (AMs) are engineered structures consisting of subwavelength unit cells that possess extraordinary abilities to control sound waves that are not found in conventional materials. These abilities allow AMs to be designed as acoustic absorbers, barriers, lenses and cloaks [1], [2], [3]. Acoustic metamaterial lenses are designed to guide and focus acoustic waves onto the desired focal points. Among them, acoustic Luneburg lenses are radially symmetric gradient refractive index (GRIN) metamaterials, which curve the incident plane acoustic waves to the focal point on the boundary of the lens. These devices have potential applications in industrial fields for non-destructive testing and imaging and in medical fields for therapeutic and imaging devices [4]. Using acoustic metamaterial lenses for ultrasound applications require them to perform well in underwater background medium, as water is the best medium for ultrasound wave to propagate without loss. In recent years, researches focused on designing acoustic metamaterial lenses for ultrasound applications and underwater environments. In the year 2020, Allam et al [5] proposed a 3D printed GRIN lens based on air inclusions inside a polymer for the working frequency of 100 kHz. The impedance difference needed for each unit cell's refractive index was achieved by changing the filling fraction of trapped air inside the polymer matrix. The unit cells showed strong anisotropy which limits the applications of this lens. This study investigated the idea of changing the material of the lens from PLA to another material with pressure-wave speed matched to water and much lower shear-wave speed and reported that the new lens outperformed the lens made from PLA. Due to the importance of this study, more of it will be explored in the next sections. In a study form 2022, Kim et al [6] introduced metallic cross shaped unit cells to form the spherical and ellipsoidal omnidirectional acoustic metamaterial lenses for working frequencies of 60 to 160 kHz. The lenses were made of stainless steel with a much higher wave speed than water and made the needed impedance difference possible for a GRIN lens. However, this choice for unit cells was reported as being not economic, difficult to fabricate and bulky which made commercializing the lenses challenging. In 2023, Tong et al [7] designed and fabricated a 3D gradient face-centered-cubic phononic crystal. This structure had quasi-isotropic refractive index profile and was fabricated with photosensitive resin by additive manufacturing techniques. This lens seemed difficult to fabricate, but provided omnidirectional imaging of underwater acoustic waves in working frequencies of 30 to 38 kHz. The effectiveness of this structure was validated by quasi-2D simulations and experimental investigations. Recent studies have focused on improving the performance of acoustic Luneburg lenses through optimization methods. One work analyzed the acoustic gain to determine conditions for maximum efficiency [8], while another developed optimized 2D underwater lenses with low directivity [9]. In contrast, the present study does not aim to optimize lens geometry or parameters but rather compares the performance of lenses made from four different commonly used polymers, providing a practical evaluation of material effects in underwater conditions.

Material properties, like density, elastic modulus and Poisson's ratio, are important in overcoming the challenges of an underwater medium. These parameters influence the acoustic impedance and refractive indices of unit cells, as well as overall performance of the lens. However, most of the existing research focused on new designs of acoustic metamaterial lenses. As additive manufacturing technologies have become the major technique to manufacture GRIN lenses, this study investigates the effect of choosing between commonly available polymers used in these printers. Therefore, four underwater acoustic Luneburg lenses using four different materials (PLA, ABS, PETG and Nylon) for the ultrasound frequency of 40 kHz are designed. Numerical simulations in COMSOL are used for deriving dispersion curves, refractive indices of unit cells and evaluating the performance of these lenses. Section 2, explains the design process and section 3 provides the simulation procedure and results of this numerical study. Conclusion and key findings are presented in section 4.

2. Design Principles

This section covers the principles used in the design process of four acoustic metamaterial lenses. First, the acoustic Luneburg lens is introduced, then the unit cells design procedure is presented. At last, unit cells' arrangement according to the Luneburg lens profile to form the lens structures is discussed.

2.1 Acoustic Luneburg Lens

GRIN lenses are a special type of acoustic metamaterial lenses which make acoustic focusing possible by varying the refractive index across the structure. This enables lenses to curve the incoming waves in a desired direction and focus these waves in the predetermined focal points. Luneburg lenses which were originally introduced in optics [10], are a subset of GRIN lenses and have a radially symmetric refractive index profile. This profile causes the incoming plane waves to be focused at a point on the boundary of the lens as shown in Figure 1(a). The governing equation of the modified Luneburg lens refractive index profile, which empowers the ability of changing the focal point's location is presented as follows [11]:

$$n(r) = \frac{\sqrt{F^2 + R^2 - r^2}}{F} \tag{1}$$

in which n is the refractive index, r is the radial distance from the centre of the lens, F is radial location of the focal point and R is the radius of the lens.

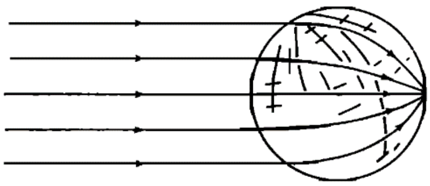

(a) Focusing plane waves at a point on the surface of the lens [12].

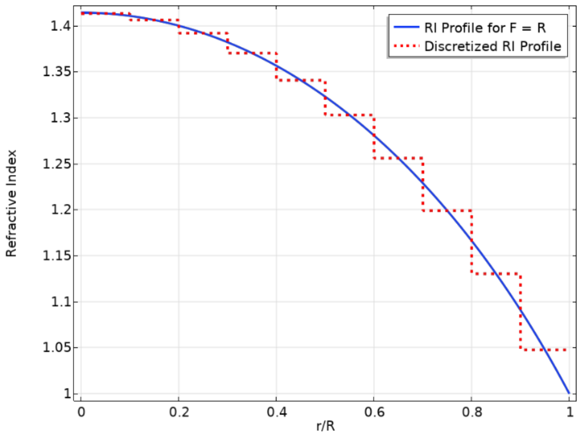

(b) Luneburg's continuous and discretized refractive index (RI) profile for $F = R$.

Figure 1. Acoustic Luneburg lens.

The refractive index profile for the general case of Luneburg lens ($F = R$) is shown in Figure 1(b). This profile is discretized in 10 layers and acoustic metamaterials are proposed as structures which are capable of establishing this discretized profile.

2.2 Material-Based Unit Cell Design

Cubic polymer unit cells with trapped air (shown in Figure 2(a)) are chosen as unit cells for this study [5]. The contrast in density and sound speed between air and water creates the necessary acoustic impedance difference within the unit cells, enabling control of the refractive index by varying the air volume inside each cell. The polymer can be considered as the background medium for the lens alongside water because of its close impedance to water. For this reason, Periodicity ($d = 3\ mm$) is fixed in this design and the air volume inside each unit cell is changed by varying the proposed filling factor (denoted by a). However, the question arises when there is a choice to be made about the material of the lens. The use of polymer background has a major difference with water background. As there is no shear wave propagation in fluids, the shear waves propagation should be accounted for in the solid medium. This requires the consideration of both material and geometry of the unit cells as well as the entire lens structure because these hold the parameters that define the acoustic wave field [5]. While the unit cells and lens geometry are fixed to be a cube, the focus of this study is to investigate material's affect.

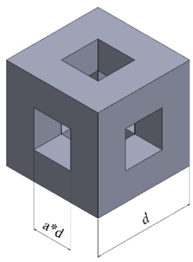

(a)

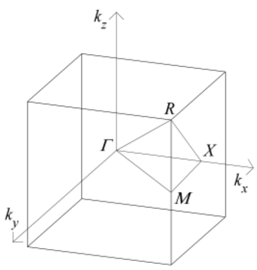

(b)

Figure 2. (a) Unit cell design and (b) irreducible Brillouin zone used for calculating dispersion curves.

In order to arrange unit cells next to each other and form the lens, the refractive indices of these cells with different air volumes should be calculated. Refractive indices are a sub result of calculating the dispersion curves. These curves which are relating the frequency in time domain (f) to frequency in space domain (wave number k), show how waves propagate through a structure. Deriving these relations is done by solving an eigenvalue problem resulting from employing Floquet-Bloch answer in the wave equation. The wave equation for elastic wave propagation in a solid material is presented as [13]:

$$\nabla.(C:\nabla\vec{u}) = \rho\frac{\partial^2\vec{u}}{\partial t^2} \quad (2)$$

where C is the stiffness tensor, $\vec{u}$ is the displacement vector, and ρ is the density of the material. The Floquet-Bloch theorem, gives a solution to the wave equation in periodic structures and is as follows [14]:

$$\vec{u}_k(\vec{r},t) = Re\left[\vec{u}_k(\vec{r})e^{-i\omega(\vec{k})t}\right] \quad \text{where} \quad u_k(\vec{r}) = f_k(\vec{r})e^{i\vec{k}.\vec{r}} \quad (3)$$

in which $\vec{r}$ and t denote the position vector and time, respectively. $\vec{k}$ is the wave vector and ω is angular frequency. The function $f_k(r)$ is a periodic vector function with the same spatial periodicity as the structure. An eigenvalue problem arises by substituting Eq (3) into Eq (2). Solving the eigenvalue problem, results in the dispersion relation $\omega = \omega(\vec{k}) = \omega(k_x, k_y, k_z)$. The dispersion relation is calculated in the ΓX direction within the irreducible Brillouin zone (shown in Figure 2(b)) of the reciprocal space $(\overrightarrow{k_x}, \overrightarrow{k_y}, \overrightarrow{k_z})$, which contains all the unique wave propagation information due to symmetry, making it unnecessary to compute the relation over the entire unit cell. This method is first applied to the simple cubic cells of four materials to evaluate their pressure and shear wave speeds (the slope of dispersion curves) and the results are then compared to theoretical values. PLA, ABS, PETG and Nylon as commonly available 3D printing materials are chosen for the purpose of this study and their estimated properties by the provider are presented in Table 1. The dispersion diagrams for each material are calculated and shown in Figure 3(a). As seen in this figure, for the case of wave propagation in ΓX direction, there are three fundamental modes for each material in these diagrams. The first two modes are the equal and overlapping shear modes in the yz plane, while the third mode is the pressure wave mode in the x direction. This is also shown in Figure 3(b-e) for further clarification. Theoretical pressure (c_p) and shear wave (c_s) speeds in solid materials are given by [15]:

$$c_p = \sqrt{E(1-v)/\rho(1+v)(1-2v)} \quad (4)$$

$$c_s = \sqrt{E/2(1+v)\rho} \quad (5)$$

Table 1. Pressure wave and shear wave speeds in chosen materials derived by two methods (E is the elastic modulus, ρ is the density and v is Poisson's ratio of the material).

Material	Properties	Method	Pressure Wave Speed (c_p in m/s)	Shear Wave Speed (c_s in m/s)
PLA	$E = 3.6\ GPa, \rho = 1250\ kg/m^3, v = 0.36$	Theory	2.2001×10^3	1.0290×10^3
		COMSOL	2.2001×10^3	1.0290×10^3
ABS	$E = 2\ GPa, \rho = 1040\ kg/m^3, v = 0.38$	Theory	1.8974×10^3	8.3472×10^2
		COMSOL	1.8974×10^3	8.3475×10^2
PETG	$E = 2.2\ GPa, \rho = 1250\ kg/m^3, v = 0.4$	Theory	1.9420×10^3	7.9282×10^2
		COMSOL	1.9419×10^3	7.9278×10^2
Nylon	$E = 2.7\ GPa, \rho = 1050\ kg/m^3, v = 0.35$	Theory	2.0315×10^3	9.7590×10^2
		COMSOL	2.0314×10^3	9.7605×10^2

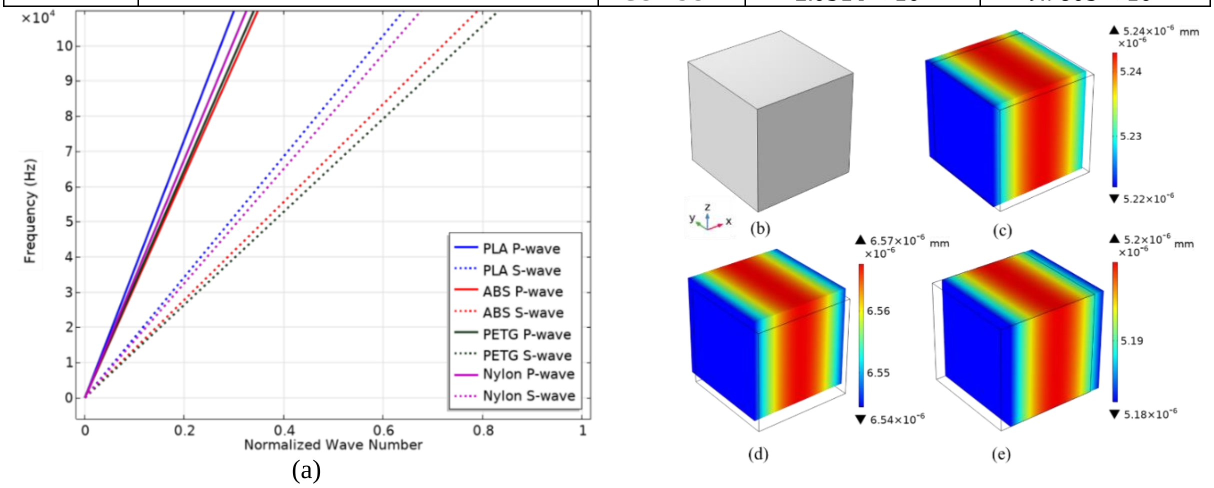

Figure 3. (a) Dispersion diagrams of cubes with different materials, (b) the simple cube which is chosen to study wave propagation in materials, (c) Shear wave mode propagating in the yz plane with a dominant displacement component along the y-direction, (d) Shear wave mode propagating in the yz plane with a dominant displacement component along the z-direction, and (e) pressure wave mode inside the PLA cube.

Comparison of the numerical and theoretical methods to achieve the wave speeds is done in Table 1. The good agreement between theory and COMSOL values verifies the method used in the numerical simulations. It is shown that PLA has the highest-pressure wave speed while ABS has the lowest. It is also of interest to note that PETG has the lowest shear wave speed amongst these materials.

Based on the steps stated above, the procedure of deriving dispersion curves is done for unit cells with different air inclusions. Two examples of the PLA unit cells' curves are derived and compared with the results from Allam's study [5] in Figure 4. The results show good agreement, although the deviations are from the difference between filling factors in the two study. The filling factor in this article is the length of the air inclusion and in Allam's study was the fraction of air volume to PLA volume (ϕ). The dispersion diagrams for each material are shown in Figure 5. The discontinuities which are shown in some curves (for example at $a = 0.775$ in PLA) are due to mode conversions in corresponding frequencies.

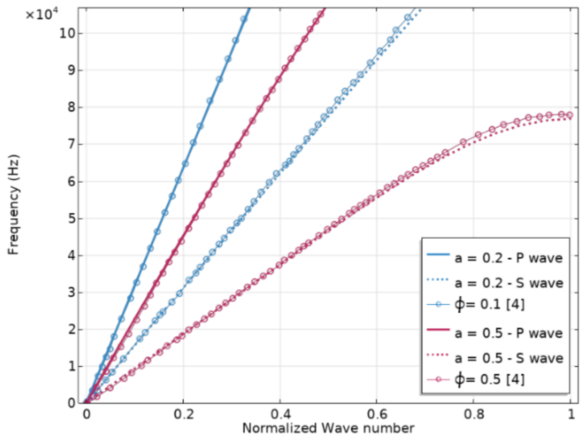

Figure 4. Verification of PLA unit cells dispersion curves.

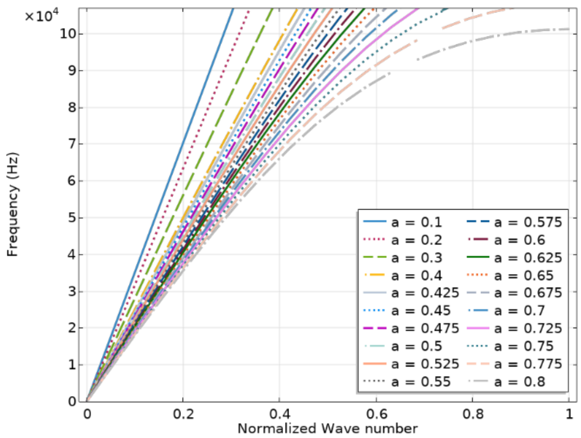

(a) PLA

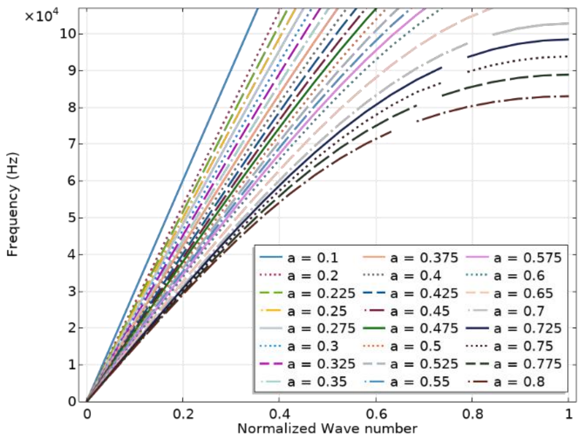

(b) ABS

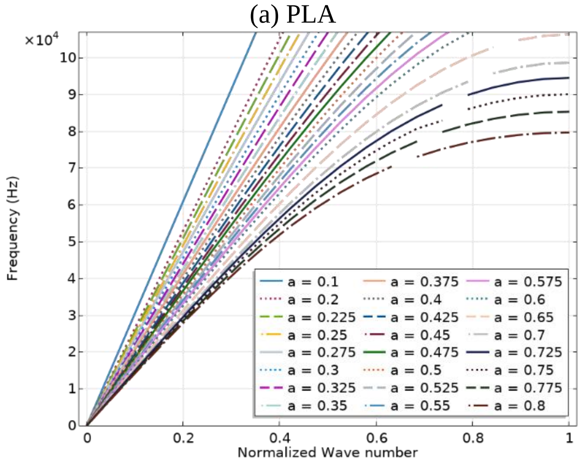

(c) PETG

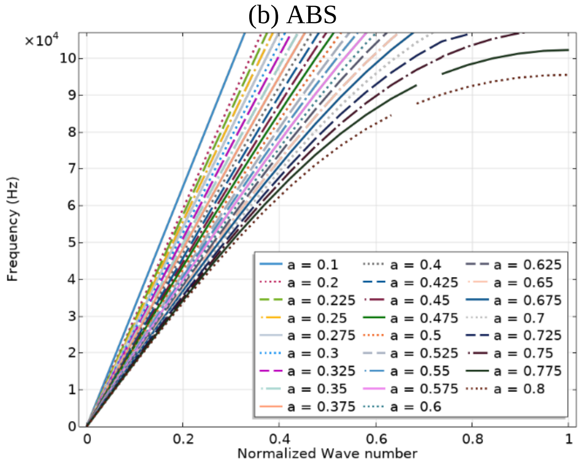

(d) Nylon

Figure 5. Dispersion diagrams of the unit cells for four materials.

Pressure wave speeds in ΓX direction in each unit cell is the one needed for the refractive index derivation. The refractive index can then be calculated using:

$$n = c/c_{\Gamma X} \tag{6}$$

in which $c_{\Gamma X}$ is the pressure wave velocity in the ΓX direction of the unit cell and c is the reference phase velocity of the pressure wave in water. The result is shown in Figure 6. As the refractive indices from 1 to 1.41 are of importance in realizing the general Luneburg lens profile, the filling factors are chosen in a way to better provide this requirement. Wide range of refractive index is available at a broadband frequency to work with, which allows for precise implementation of the Luneburg lens profile. Working frequency of 40 *kHz* is chosen for designing the four mentioned metamaterials.

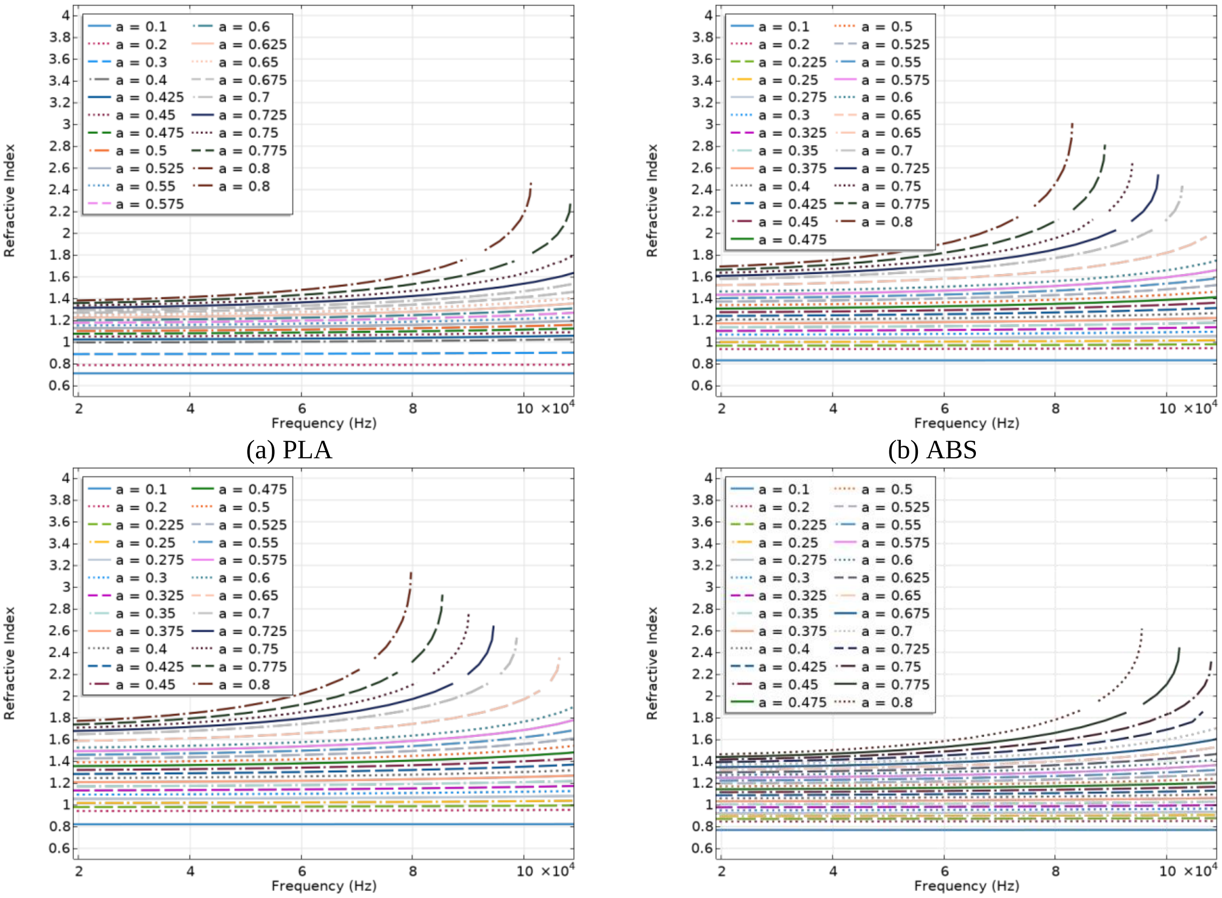

(a) PLA (b) ABS

(c) PETG (d) Nylon

Figure 6. Refractive index diagrams of the unit cells for four materials.

2.3 Arrangement of Unit Cells in Metamaterials

Based on the refractive index diagrams and in order to achieve the refractive index profile of the general case of the Luneburg lens ($F = R$) with the metamaterials, Table 2 is presented. The four lenses are considered to be discretised in 10 layers. This table depicts the needed refractive indices in each of the 10 layers of the metamaterials. Also, it shows the closest refractive index of various material's unit cells with different filling factors at the working frequency of 40 *kHz*. The table covers all four materials of PLA, ABS, PETG and Nylon. It can be seen that it is possible to achieve the needed refractive index of Luneburg lens in each layer with these materials with a low deviation percentage (max = 1.5005 % for Nylon). Providing accurate refractive index values in each layer is necessary in implementing a GRIN lens. As shown by the table nearly the same value of the refractive index is successfully achieved by each material. The unit cells made of ABS and PETG have lower filling factors than PLA and Nylon, meaning they can provide the needed refractive index with lower volume of air inclusions.

Four aforementioned lenses are created by a careful arrangement of unit cells next to each other in 10 layers to create the discretized Luneburg lens profile as shown in Figure 7. In order to achieve minimum reflections from the edges, a square lens is introduced. The surrounding unit cells of the 10th layer are chosen in a way to produce a refractive index equal to 1, so that there is minimum reflection of the acoustic waves when they enter the metamaterial. Also, a complementary part of 0.2 mm thickness of the same material is designed and assembled to outer boundaries of each lens, so that water does not penetrate the structure. This 2D lens design is extendable to a 3D spherical and cubical design, while itself is valuable in various cases of practical real-world applications.

Table 2. Refractive indices of unit cells of different filling factors

Layers	Luneburg RI	PLA		ABS		PETG		Nylon	
		a	RI	a	RI	a	RI	a	RI
1	1.4133	0.8	1.4122	0.55	1.4136	0.5	1.3991	0.725	1.4121
2	1.4062	0.8	1.4122	0.55	1.4136	0.5	1.3991	0.7	1.3851
3	1.3919	0.775	1.3821	0.525	1.3807	0.5	1.3991	0.7	1.3851
4	1.3702	0.775	1.3821	0.525	1.3807	0.475	1.3635	0.675	1.3588
5	1.3407	0.75	1.3557	0.5	1.3465	0.45	1.3261	0.65	1.3330
6	1.3029	0.7	1.3048	0.475	1.3135	0.425	1.2881	0.625	1.3073
7	1.2560	0.65	1.2562	0.425	1.2443	0.4	1.2496	0.575	1.2548
8	1.1990	0.6	1.2073	0.4	1.2090	0.375	1.2114	0.525	1.2010
9	1.1303	0.525	1.1310	0.35	1.1381	0.325	1.1337	0.45	1.1180
10	1.0476	0.45	1.0517	0.275	1.0331	0.275	1.0548	0.4	1.0608
Maximum Deviation %		1.1188%		1.3841%		1.1359%		1.5005 %	

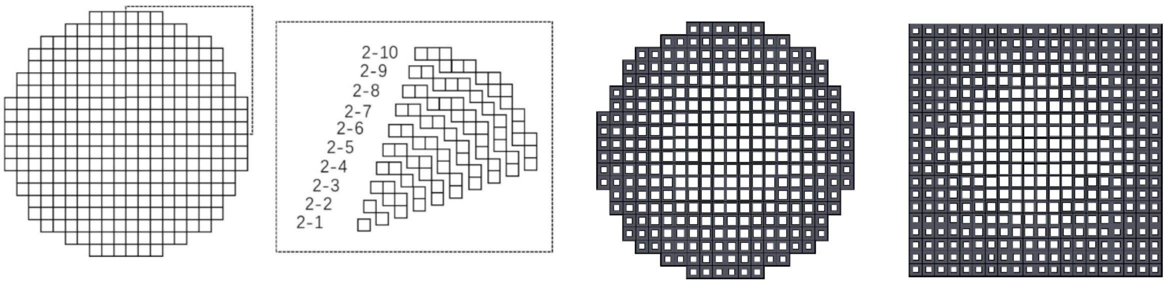

(a) Discretized lens[16] (b) PLA Lens (c) PLA Square Lens

Figure 7. Discretized lens in 10 layers and example of the completed lens design of PLA material.

3. Simulations and Results

The four designed lenses are modelled by SOLIDWORKS software and then are implemented into the COMSOL Multiphysics software for performance analysis. The simulations are performed using the acoustic-structure multiphysics with the coupling between transient pressure acoustics and solid mechanics modules. With these assumptions, the wave equations in both fluid and solid domain are solved simultaneously. The lenses (modelled with solid mechanics module) are placed in the middle of the rectangular block domain of $300 \times 150 \times 3\ mm^3$ which is used to model the surrounding water (modelled with pressure acoustics, transient module). Due to weak coupling of acoustic waves in the air and polymer background because of the large impedance mismatch, acoustic waves in air do not take part in pressure wave propagation. So, the air inclusions inside unit cells are modelled as free boundary condition. Periodic boundary conditions are used in top and bottom surfaces of the lens and background medium to create a quasi 2D environment. Perfectly matched layers of adequate sizes are used around the boundaries of the water domain so that the waves are not reflected back to the domain from the boundaries. A mesh with at least 10 elements per wavelength is used to discretize the simulation environment. Water's density and speed of sound are considered to be $1000\ kg/m^3$ and $1500\ m/s$ respectively. Material properties of PLA, ABS, PETG and Nylon are provided in Table 1. Background pressure filed with $1\ Pa$ amplitude and working frequency of $40\ kHz$ is considered in the fluid domain. A total simulation time of $1000\ \mu s$ is chosen to ensure the acoustic wave has enough time to travel the simulation domain, interact with the metamaterial and stabilize the focal point in the wave field. Also, a time step of $1\ \mu s$ is chosen for the $40\ kHz$ sound wave, as the period of this wave is $25\ \mu s$ and at least 25 time steps per cycle is ensured by this choice. The results are shown at $1000\ \mu s$ in this section.

The results from the numerical simulations of the acoustic metamaterial Luneburg lenses designed of four materials are presented in Figure 8 and Figure 9. The acoustic intensity and pressure are shown along the y axis in Figure 8 which is perpendicular to the focal axis, also the intensity filed is presented for each lens in Figure 9. Among the four metamaterials, Nylon lens has the highest focal intensity and pressure amplification with 2.752 times the incident pressure amplitude. The PLA-based lens has lower peak intensity and pressure with 2.5712 times the incident pressure amplitude. This is due to better impedance matching of Nylon, because of its closer density to water and its lower shear wave speed than PLA as their pressure wave speeds are close to each other. On the other hand, PLA lens has a full width at half maximum (FWHM) of 0.5723λ which is narrower than Nylon lens with 0.6593λ. This indicates better wave confinement of PLA than Nylon. However, both have well wave focusing with a FWHM lower than 0.7λ. These findings indicate that choosing between PLA and Nylon should be done by considering the needed application to balance between focal intensity and FWHM. Both of these lenses exhibit strong side lobes due to the diffraction of waves around the edges of the rectangular lens. These secondary peaks indicate that while intended focal points are formed correctly, edge diffractions have a significant role in distributing waves outside the focal points. Higher intensity focal point of Nylon lens is achieved with the cost of higher intensity side lobes around the edges than PLA lens.

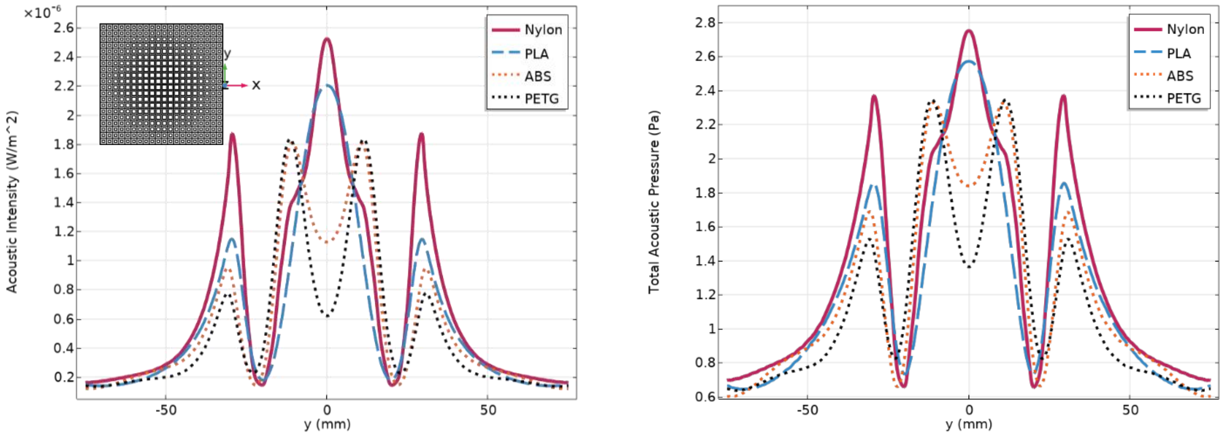

(a) Intensity profile (b) Pressure profile

Figure 8. Intensity and pressure diagrams of the four acoustic metamaterial Luneburg lenses

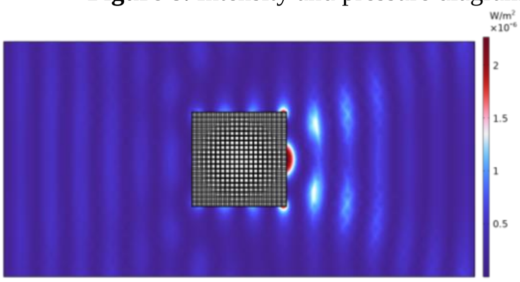

(a) PLA

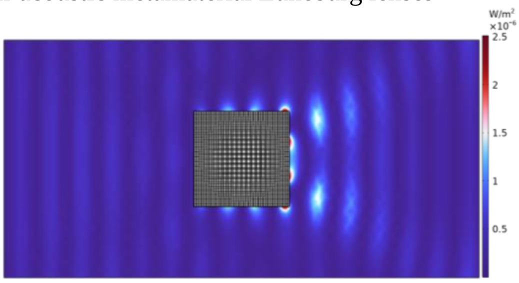

(b) ABS

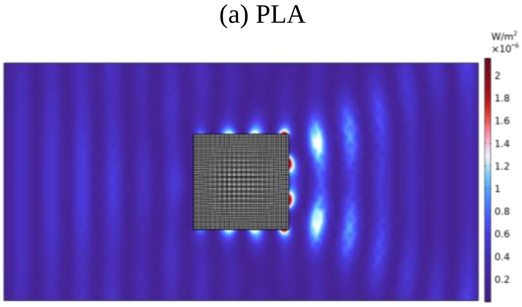

(c) PETG

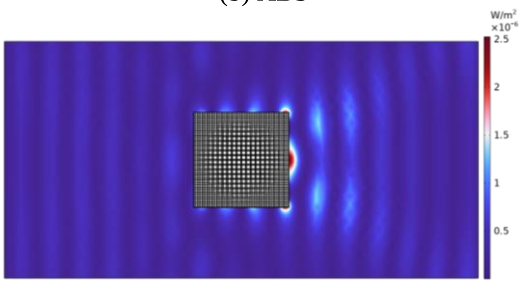

(d) Nylon

Figure 9. Intensity distribution of the four acoustic metamaterial Luneburg lenses.

The ABS and PETG-based lenses do not produce the intended focal point. These materials generate four lobes. Two of these side lobes are due to edge diffraction of waves. But, two side lobes are on either side of the focal region and are $21.4690\ mm$ apart from each other for ABS and $22.7740\ mm$ apart for PETG. The focal point produces a pressure amplification of 1.8393 times the incident wave for ABS and 1.3636 times for PETG. As the refractive indices of these lenses are implemented with minimum errors, the possible deviation from the refractive index profile is not considered as a reason for this behaviour. However, they are not accepted as acoustic metamaterial lenses because their focal point is not pre designed and the acoustic energy is distributed into multiple regions.

4. Conclusion

This study presents the design and simulation of four acoustic metamaterial Luneburg lenses made from common 3D-printing materials of PLA, ABS, PETG and Nylon. The metamaterials were constructed by cubic unit cells with trapped air inclusions. Calculation of unit cells' dispersion diagrams was performed numerically and wide ranges of refractive indices resulted for each material. Unit cells were arranged based on the discretized general Luneburg lens refractive index profile to form the metamaterials. Performance analysis was performed by numerical simulations to derive focal intensities, pressure amplifications and FWHMs of all four acoustic lenses. The results demonstrate that Nylon and PLA based acoustic lenses successfully achieved strong focal intensities and pressure amplifications in the predetermined focal point. Nylon produced the higher pressure peak of 2.752 times the incident amplitude, while PLA had a narrower FWHM of 0.5723λ. However, both lenses produced side lobes at the edges of the rectangular lens due to edge diffractions. This can be minimised by optimizing the lens shapes. To select between one of these lenses, their amplifications and FWHMs should be considered based on the specific application in mind. On the other hand, the lenses based on ABS and PETG failed to produce the intended focal points and instead created multiple focal regions. Two of these regions appeared symmetrically around the focal point region. ABS and PETG based lenses were not proposed as acoustic metamaterial lenses as they produced unintended focal regions. These results conclude the material-based comparative design of the acoustic metamaterial Luneburg lenses by highlighting the importance of selecting the right material for achieving precise acoustic focusing.

REFERENCES

[1] G. Liao, C. Luan, Z. Wang, J. Liu, X. Yao, and J. Fu, "Acoustic Metamaterials: A Review of Theories, Structures, Fabrication Approaches, and Applications," *Adv. Mater. Technol.*, vol. 6, no. 5, pp. 1–29, 2021, doi: 10.1002/admt.202000787.

[2] G. Aydın and S. E. San, "Breaking the limits of acoustic science: A review of acoustic metamaterials," *Mater. Sci. Eng. B*, vol. 305, no. January, p. 117384, 2024, doi: 10.1016/j.mseb.2024.117384.

[3] G. Comandini, M. Ouisse, V. P. Ting, and F. Scarpa, "Architected acoustic metamaterials: An integrated design perspective," *Appl. Phys. Rev.*, vol. 12, no. 1, 2025, doi: 10.1063/5.0230888.

[4] L. Zhao, C. Bi, H. Huang, Q. Liu, and Z. Tian, "A review of acoustic Luneburg lens: Physics and applications," *Mech. Syst. Signal Process.*, vol. 199, no. November 2022, p. 110468, 2023, doi: 10.1016/j.ymssp.2023.110468.

[5] A. Allam, K. Sabra, and A. Erturk, "3D-printed gradient-index phononic crystal lens for underwater acoustic wave focusing," *Phys. Rev. Appl.*, vol. 13, no. 6, p. 1, 2020, doi: 10.1103/PhysRevApplied.13.064064.

[6] J. W. Kim, G. Hwang, S. J. Lee, S. H. Kim, and S. Wang, "Three-dimensional acoustic metamaterial Luneburg lenses for broadband and wide-angle underwater ultrasound imaging," *Mech. Syst. Signal Process.*, vol. 179, no. March 2022, p. 109374, 2022, doi: 10.1016/j.ymssp.2022.109374.

[7] S. Tong and C. Ren, "3D underwater acoustic Luneburg lens based on gradient face-centered-cubic phononic crystals," *Appl. Phys. Lett.*, vol. 123, no. 3, 2023, doi: 10.1063/5.0145179.

[8] A. Ricardo and V. M. Duarte, "Towards an optimal design of acoustic Luneburg lenses," vol. 2219, no. November 2021, pp. 2211–2219, 2024, doi: 10.1121/10.0030405.

[9] S. Cominelli and F. Braghin, "Optimal design of broadband, low-directivity graded index acoustic lenses for underwater communication," *J. Acoust. Soc. Am.*, vol. 156, no. 3, pp. 1952–1963, 2024.

[10] R. K. Luneburg, "Mathematical Theory of Optics," 1966.

[11] L. Zhao, T. Horiuchi, and M. Yu, "Broadband acoustic collimation and focusing using reduced aberration acoustic Luneburg lens," *J. Appl. Phys.*, vol. 130, no. 21, 2021, doi: 10.1063/5.0064571.

[12] C. A. Boyles, "Wave Theory of an Acoustic Luneberg Lens," *J. Acoust. Soc. Am.*, vol. 43, no. 4, pp. 709–715, 1968, doi: 10.1121/1.1910886.

[13] W. S. Gan, *New acoustics, based on metamaterial*, vol. 15. 2012. doi: 10.1121/1.4764497.

[14] G. Yi and B. D. Youn, "A comprehensive survey on topology optimization of phononic crystals," *Struct. Multidiscip. Optim.*, vol. 54, no. 5, pp. 1315–1344, 2016, doi: 10.1007/s00158-016-1520-4.

[15] O. T. Bruhns and O. T. Bruhns, *Advanced mechanics of solids*. Springer, 2003.

[16] "Broadband underwater acoustic lens based on five-mode microstructure and optimization method," vol. 29, no. 19, 2022.